Ageing estimation of lithium-ion batteries applied to a three-wheel PHEV roadster

Nadeau J. / Dubois M. R. / Desrochers A. / Denis N.
Centre de technologies avancées BRP - Université de Sherbrooke
University of Sherbrooke
Sherbrooke (Quebec), Canada
jonathan.nadeau@cta-brp-udes.com

***Abstract*—Predicting the ageing behaviour of a lithium-ion battery is a challenging difficulty in plug-in hybrid electric vehicles applications. Invoking the expensive price of the energy density linked with considerable performances degradation over cycling, it is worth considering a battery lifetime optimization in the design process. The degradation will materialize by a capacity loss and an increase of the internal resistance. Capacity loss will affect the autonomy of the vehicle while an increase of the internal resistance will lead to an increase of the battery power losses and overheating. In the paper, the lifetime of a PHEV roadster battery pack is estimated by applying a real-life current discharge pattern, instead of the common ageing experiments based on constant current discharge patterns. A current cycle corresponding to a roadster power load has been used as input. This work involves an accelerated ageing experiment of individual LiFePO$_4$ battery cells through cycling. The cycle applied is derived from a speed cycle comprised of three parts: urban roads, rural roads and highways. For more than 1400 cycles, the capacity, internal resistance, voltage, current and temperature have been monitored.**

Keywords— ageing; lifetime; lithium-ion; batteries; capacity fading; internal resistance growth; PHEV; automotive

I. INTRODUCTION

There is a need for alternative energies in automotive applications. Over the past 20 years, there have been sustainable improvements in the industry of hybrid electric vehicles (HEV). However, a significant barrier still making HEV less attractive than gasoline vehicles is the high price of the batteries. Also, the lack of knowledge about the ageing behaviour of the batteries will often impact the dissemination of such vehicles negatively. Nowadays, it is well recognized by the automotive community that Li-ion, especially $LiFePO_4$, is a chemistry offering one of the best performances, for both EV and plug-in hybrid electric vehicle (PHEV) applications [1].

Thus, the Centre de technologies avancées (CTA) is considering this kind of technology for the hybridization of a three-wheel roadster, for which space allocation for the battery pack is an important restriction. As a consequence of the small battery space requirement, the battery solicitation is well above common hybrid automotive applications. In this context, the battery will need to sustain high currents, significant temperature rise and deeper discharge which, according to [2], [3] and [4], will accelerate the battery ageing process. Moreover, [5] has shown that the current pattern (constant or peaky) will also have an impact on the ageing mechanism of the battery. This ageing will materialize by the capacity fading and the internal impedance growth, which have a direct impact on the vehicle performances (Fig. 1). In the case of a sport PHEV roadster, the aggressive power demand will be more stringent on the battery. Thus, accurate lifetime prediction is mandatory, even more so than for common PHEV designs.

This paper focuses on the Li-ion battery lifetime estimation applied to a PHEV roadster by using a typical motorcycle reference speed cycle which is known as the Worldwide Motorcycle Test Cycle (WMTC). The lifetime prediction established in the paper is based on a repeated power cycle application on four independent $LiFePO_4$ battery cells. The battery current pattern will be extracted from the vehicle power cycle output, coming from a roadster powertrain simulation. Assumptions will be made on the hybrid control strategy, from [6], regarding the power exchange management between the internal combustion engine (ICE), the electric motor and the battery pack. During the experimental ageing process performed in laboratory, the capacity loss and the internal resistance growth through cycling were observed. In this paper, the methodology adopted to obtain the battery pack electric power demand, including the modelling of the powertrain, is first explained. Then, the experimental protocol will be described, followed by a discussion of the results and the lifetime prediction made from them.

II. HYBRID ROADSTER MODELING AND ELECTRIC POWER DEMAND CALCULATION

A simulator for a three-wheel PHEV roadster has been developed by the CTA [6]. It features the powertrain model computation (electrical modelling and mechanical modelling), which considers the effects of the aerodynamic drag and the rolling resistance. The input for this model is the vehicle speed imposed by the WMTC speed cycle, as shown in fig. 4.

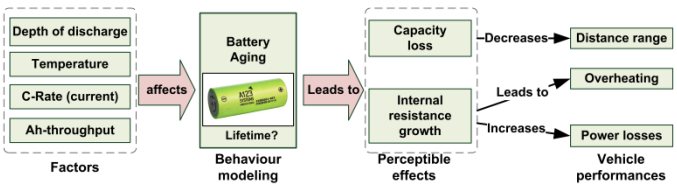

Fig. 1. Ageing behaviour of a Li-ion battery in an automotive application

A. *Electric model of the powertrain*

The electric powertrain model includes a battery pack made with $LiFePO_4$ cells, an inverter (IGBT) and an electric motor (permanent-magnet synchronous motor or PMSM). The empirical model of the battery pack developed by [7] is based on an equivalent electric circuit. It provides the bus voltage V_{bus}, as a function of the state of charge (SOC) and the output current, taking into account the effects of the temperature. The PMSM model considers the hysteresis losses, eddy current losses and copper losses. Finally, the inverter model computes the conduction losses and switching losses [6].

Considering the simplified powertrain architecture of Fig. 4, the battery pack power demand is defined as the sum of the PMSM power load, the total power losses (inverter, PMSM, battery pack, etc.) and the power provided to the accessories (e.g. lights, HMI, pumps):

$$P(t)_{batt} = P(t)_{PMSM} + P(t)_{loss} + P(t)_{acc}\,. \tag{1}$$

B. *From a speed cycle to an electric power cycle*

Assuming a flat road, the longitudinal propulsion force F_{mec} is calculated so that the vehicle speed (m/s) is met at all time during the WMTC cycle. Using the three wheels roadster's free body diagram of Fig. 2, the forces considered are: the aerodynamic drag (F_d) and the rolling resistance (F_{rr}), which is related to gravity:

$$m\dot{v} = \sum F = F_{mec} - F_d - F_{rr} \tag{2}$$

where forces are defined as:

$$F_d = 1/2\sigma C_d A v^2 \tag{3}$$

$$F_{rr} = C_{rr1} mg + C_{rr2} mgv + C_{rr3} mgv^2 \tag{4}$$

and parameters definitions are:

Fig. 2. Free body diagram of the hybrid three wheels roadster.

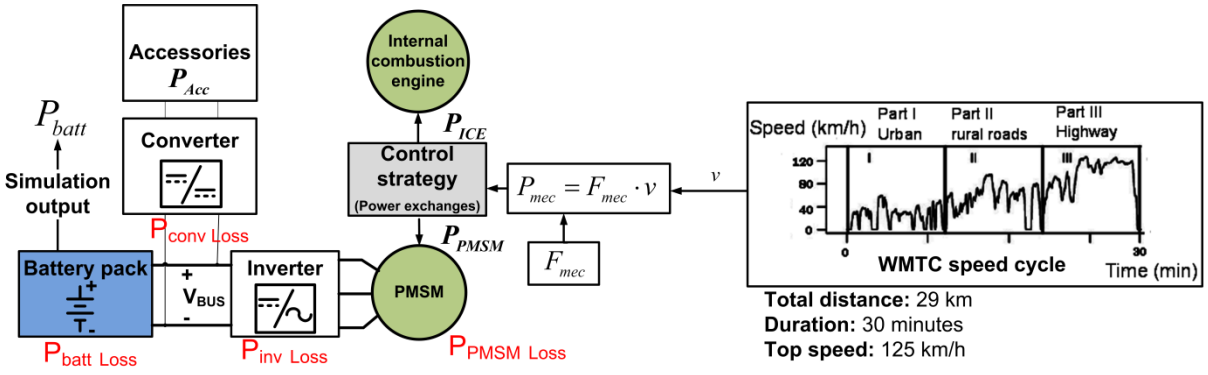

Fig. 4. The simplified three wheel PHEV simulator architecture.

- m the mass of the vehicle (kg);
- ρ the density of the air (kg/m^3);
- C_d the aerodynamic drag coefficient;
- A the front area of the vehicle (m^2);
- C_{rrx} the rolling resistance coefficient.

Finally, the total power demand is obtained as:

$$P_{mec} = F_{mec} \cdot v = P_{PMSM} + P_{ICE}\,. \tag{5}$$

C. *The control strategy*

The PHEV roadster implements a standard parallel hybrid architecture. The propulsion torque distribution transferred to the rear wheel between the internal combustion engine (ICE) and the electric motor is managed by a control strategy developed by [6]. For the experiment, the WMTC speed cycle, which is shown in Fig 4, is considered. This is a European motorcycle test cycle, commonly used to characterize the carbon emissions for motorcycles. It includes three driving sequences: urban, rural and highway. In this work, an optimized hybrid control strategy has been used. It minimizes the overall gasoline consumption. To do so, the battery is operated in a charge depleting mode pattern (≈ 22 min), which is then followed by a charge sustaining mode for the remaining 8 minutes of the cycle (see Fig. 3). Thus, the contribution of the ICE controlled by the charge sustaining strategy is allowed

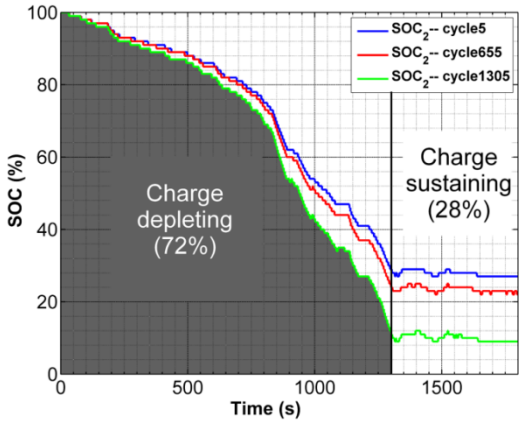

Fig. 3. SOC evolution of a cell at the beginning of its life, at mid-life and end of life over the WMTC cycle with the hybrid control strategy described.

at the end of the cycle only (highway part). This is required because of the insufficient 2kWh roadster's embedded battery pack energy to complete the entire WMTC.

The regenerative braking strategy has been simulated with an assumption of 40% kinetic energy recovery. The computed strategy over the WMTC was applied to the power cycle at the start of the experiment and no adaptation trough cycling was done to consider ageing effects on battery performances. This fact explains the SOC curve variation over cycling on Fig. 3.

D. Calculation of a single cell power demand

To compute the power demand $P(t)_{cell}$, for a single battery cell, it is assumed that the total power is equally distributed on each cell.

Then, knowing the battery pack structure, $P(t)_{cell}$ is only function of the number of cells n_{cells} and $P(t)_{batt}$, which is given by the simulation's output:

$$P(t)_{cell} = P(t)_{batt}/n_{cells} \tag{6}$$

Finally, we obtain the current of a single cell. This is the controlled variable used for cycling:

$$I(t)_{cell} = P(t)_{cell} / V(t)_{cell} \tag{7}$$

where discharge current is positive and recharge current is negative. The cell voltage $V(t)_{cell}$ is obtained by a real-time measurement during all of the experiment.

E. Performance measurement

The qualification of the battery ageing is determined by the capacity loss and the internal resistance growth [1], [8]. The first one affects the autonomy of the vehicle by decreasing the available energy, while the second one affects the power losses caused by the Joule's effect (Eq. 8). Moreover, the resistance decreases the bus voltage V_{bus} as per Eq. 9.

$$P_{bus} = P_{batt} - P_{loss} = V_{oc} I_{batt} - R_{int} I_{batt}^2 . \tag{8}$$

$$V_{bus} = V_{oc} - R_{int} I_{batt} . \tag{9}$$

The battery model proposed by [7] formulates the open circuit voltage V_{oc} as a function of the SOC, the output current I_{batt} and the temperature T_{batt}. In this work, the cell internal resistance is determined from two contributions: the ohmic resistance R_o and the polarization resistance R_p, with its associated capacitance C_p (reactance). [8] relates R_o to the electrodes material resistance, electrolytes resistance, separators resistance and contacts resistance, and R_p is associated to the electrochemical polarization and the concentration polarization. According to [8], ageing has a more considerable effect on R_o than R_p. Incidentally:

$$R_{int} = R_o + R_p \tag{10}$$

To measure the internal resistance R_{int}, the current pulse method is applied at regular time intervals during the experiment. [9] showed that the current pulse method is a good way to measure the internal DC resistance with good accuracy. The authors suggest a current pulse with a rise time of less than 100 ms, a strong current amplitude (> 10C) and a duration close to 18s.

Fig. 5 illustrates a typical voltage response obtained across the cell. This is the method used to identify the equivalent circuit model [8] shown in the same figure. The internal resistance value for R_o and R_p is calculated using Eq. 11:

$$R_{int} = (\Delta V_{R_o} + \Delta V_{R_p}) / I_{pulse} . \tag{11}$$

The cell capacity Q_{cell} is measured by using the Coulomb counting technique. It is done by integrating a constant current discharge over time, from a fully charged state to the minimal voltage permitted, defined as $V_{threshold}$, that occurs at time $t_{threshold}$:

$$Q_{cell} = \int_0^{t_{threshold}} I_{cell} dt . \tag{12}$$

F. Ageing: cycle life versus calendar life

Calendar life is not an issue in the analysis, considering the accelerated cycling ageing process adopted in the experiment. But, in real life, the analysis should include the calendar life behaviour, which has been described by [1], for Li-ion cells NNP NCR 18650 type.

III. Experimental Protocol

Four 2.3 Ah $LiFePO_4$ cells (model ANR26650m1A), manufactured by A123 systems were cycled repeatedly for more than 1400 cycles, with the same power cycle $P(t)_{cell}$, derived from the WMTC and applied to each cell.

Power electronic modules were built to apply the current cycle $I(t)_{cell}$ (Fig. 7) on each cell. Also, a complete autonomous control and data acquisition system interacting with these modules was designed. Their power electronic schematic is shown on Fig. 8.

The main protocol description is shown in table I and the associate state machine describing the repeated sequence is illustrated in Fig. 6. Note that according to [7], the current cycle will depend on the cell voltage (V_{cell}). In Fig. 7, the cell current is the image of the vehicle power. It is here expressed in C-Rate, which is defined as a ratio of the cell current in Amperes over the current value that the battery will discharge in exactly one hour:

$$C\text{-}Rate = I_{cell}\,[A]/(Q_{cell}\,[Ah]/1h). \tag{13}$$

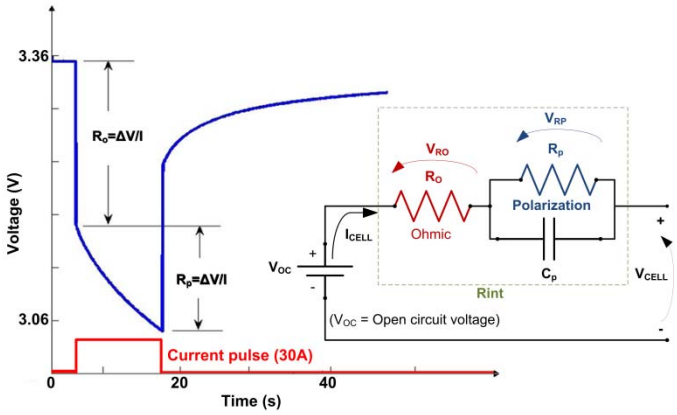

Fig. 5. Internal resistance measurement method and the considered Thevenin based battery cell equivalent circuit model for the experiment.

TABLE I. PROTOCOL DESCRIPTION FOR THE EXPERIMENT

Measures [a]	Frequency	comments
Capacity (Ah)	Every 10 WMTC discharge cycles	Complete discharge at I_{cell} =2C
Internal resistance (mΩ)	3 times for every charging event at: SOC = 30%, 70%, 90%	Current pulse method: 30 A, 15 s
Surface Temperature (°C)	Continuous (10Hz)	Ambient and not conditioned
Control		
Recharge	CCCV protocol (Constant current - constant voltage)	
Control strategy over the WMTC	Charge depleting for the first part (72%) then charge sustaining until SOC = 30%, with internal combustion engine assistance	

a. Voltage, current, temperature and SOC were monitored.

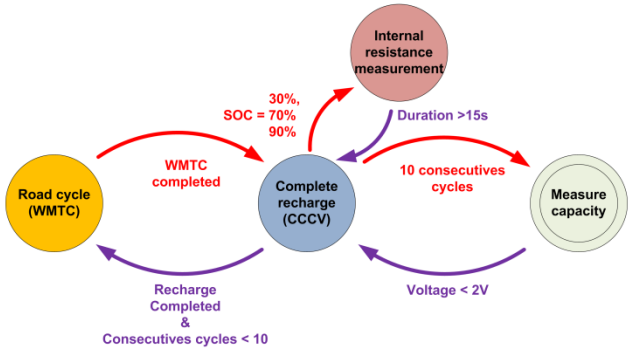

Fig. 6. State machine of the experiment sequence.

Fig. 8 shows the electrical configuration of the charge and discharge apparatus used in the experiment. A DC source of 3.6V is used for recharging the cell. This 3.6 V supply is connected in series with a P Channel MOSFET operating in linear mode to enable constant current charging. At the end of the charging period, for SOC above 80%, the P MOSFET is disabled and the cell is charged at a constant voltage of 3.6 V with the use of the SPDT relay shown at the bottom of Fig. 8.

For the discharging period, the N-Channel MOSFET shown in fig. 8 is controlled in linear mode. The MOSFET Gate voltage is adjusted by the control circuit with the objective of drawing the current as in the pattern of Fig. 7.

A. *Hardware considerations due to the design*

Due to the hardware design of each module, the following considerations have to be taken into account in the results:

In recharging mode, the saturation current of the P-MOSFET was -4.4 A, for cell sample #3. For cell samples #1, #2 and #4, it reached -8 A;

During the charging period, the threshold current between the CC and CV states was higher in cell sample #1 (-6 A instead of -3 A);

In any event, the average accuracy of the controlled current is less than 4% in both charging and discharging modes.

IV. AGEING CELLS PERFORMANCES DEGRADATION RESULTS

A. *C-Rate distribution over the cycle and its effect on ageing*

A measure of the current distribution over all of the WMTC is shown in Fig. 9. In common PHEV applications, the C-Rate effect on battery ageing can be neglected for a lifetime prediction [3], because the battery pack is usually oversized (±4C and ±2C typical). However, for this roadster application, occurrences of current peaks beyond 4C are observed 13% of the time, which will be detrimental with respect to the battery life [5].

B. *Capacity loss*

The capacity loss results are shown in Fig. 10. The end of life (EOL) resulting from a 20% capacity loss is shown in table II. It is expressed in number of WMTC cycles done and in total

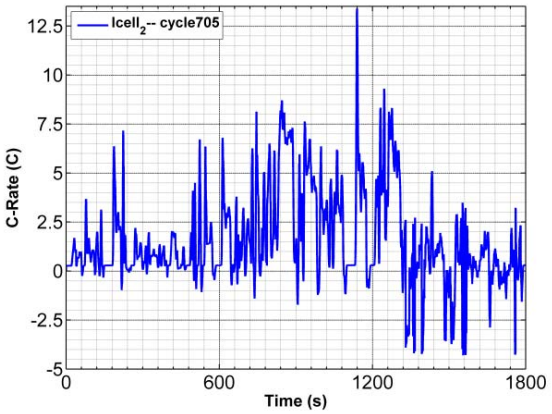

Fig. 7. Current cycle used at mid-life experiment (Cell#2 ; cycle 705).

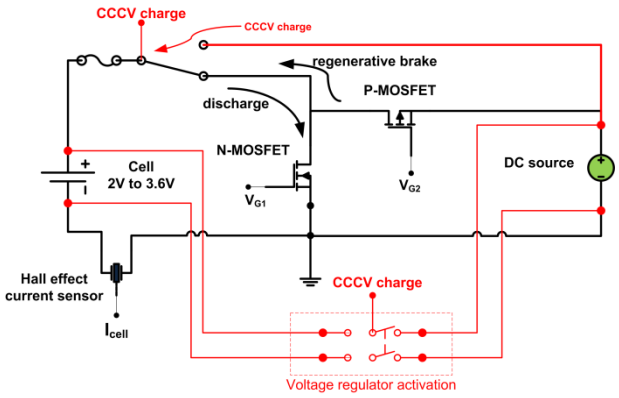

Fig. 8. Power electronic circuit used to apply the WMTC road cycle.

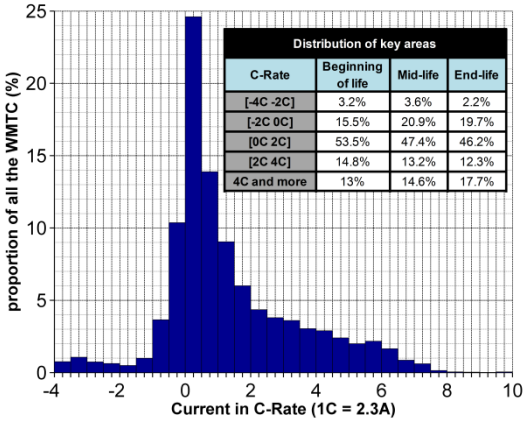

Fig. 9. Cell#2 current distribution over the WMTC at the start of the experiment.

Ah-throughput. The Ah-throughput is defined as the total electric charge exchanged by the cell including charge and discharge during its lifetime (the integral of the current over time). The EOL is reached after an average value of 1150 cycles and 5564 Ah. Cell sample #1 exhibits a faster capacity loss, with a lifetime 22% shorter than the average value. As indicated earlier, the CCCV charging hardware was setup at a higher current threshold. Obviously, harmful effects of charging aggressiveness emerge from the results. A standard deviation (σ) of 191 cycles is computed for the lifetime, which means a difference of 16.6% compared to the average value. Comparing the capacity loss results to the cell datasheet (table V), there is a 40% difference at mid-life (end-of-life is not specified). Moreover, if the battery cell empirical model of [2], which describes the capacity loss for a constant current, is compared to the number of Ah, a 12% capacity loss is expected after 5500Ah, with a constant current of 2.8 C (the RMS current computed for the WMTC cycle), which is about 40% higher in life expectation than the results obtained in this paper with the variable current pattern of fig. 7.

C. *Internal resistance growth*

The internal resistance R_o and $R_o + R_p$ of each cell was measured, at a SOC of 30%, 70% and 90%. This measurement was carried out for every recharge cycle. The internal resistance growth was then compared to the nominal values indicated in table III:

$$R_{growth}[\%] = (R_{int} - R_{nom})/R_{nom} \times 100. \qquad (13)$$

The higher percent of R_{growth} brings a higher voltage drop across the cell and is directly associated to the power losses (see Eq. 8). At the battery pack level, this will bring down the bus voltage V_{bus} proportionally. Table III and table IV show the nominal values for R_o and R_{int} (equal to $R_o + R_p$) and their respective increase measured at the beginning of life and after 1400 cycles. Fig. 11 compares the increase in the R_o value for the four cell samples tested at the same SOC value of 70%. Fig. 12 shows the increase in R_{int} for one of the cells (cell sample #2), for the three SOC at which these measurements were made. The trends and growth values of fig. 11 and 12 can be described as a 2nd degree polynomial interpolation of the measurements taken. Except for cell sample #1, a similar R_o growth trend is observed for each cell. Indeed, there is a low standard deviation (σ), of less than 3% for the three SOC. However, it is not the case for the growth of R_{int}, for which σ reaches more than 9% at a SOC=90% and is less than 6% for lower SOC values. The results also show that the increase in R_{int} is strongly dependent upon the SOC (see Fig 11). This trend also appears for R_o but in a less obvious way. Interestingly, the R_o and R_{int} decrease in value, in the first part of the ageing process. This behaviour is also described in [10].

D. *Total Ah-throughput needed for the measurements*

As mentioned earlier, the measurement of the internal resistance is done by drawing a substantial amount of current during 15 seconds, three times during the charging process. The capacity measurement also requires that the cell be discharged totally every 10 cycles. These measuring techniques bring the drawback of increasing the total number of Ah exchanged with the cell. Doing so, the measurement reported in this paper account for 24% of the total Ah-throughput cycled, i.e. 8.5% for the capacity measurement and 15.5% for the internal resistance measurement. Considering the Ah-throughput as a main ageing parameter [2], it has to be taken into account in the final lifetime estimation.

E. *Cell temperature during the experiment*

The battery cells were maintained at ambient temperature, with no additional cooling. Their surface temperature stayed in a range between 26 °C and 36 °C, during the complete course of the ageing experiment. According to the 3D map created by [7], plotting the cell internal resistance versus the SOC and temperature, this is a good range for optimal performance operation.

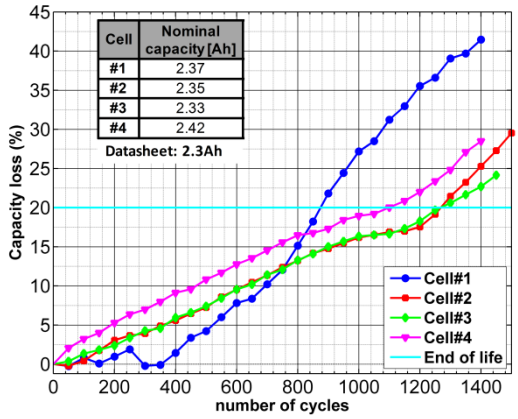

Fig. 10. Capacity loss through cycling compared to the nominal capacity.

TABLE II. END OF LIFE RESULTS FOR EACH CELL (20% CAPACITY LOSS)

	Cell #1	Cell #2	Cell #3	Cell #4
WMTC cycles	900	1300	1300	1100
Ah-throughput (Ah)[a]	4250	6267	6382	5357

b. Includes all measurements, charging and road cycles

TABLE III. NOMINAL INTERNAL RESISTANCE VALUE AT THE BEGINNING OF LIFE (R_{O_NOM}; R_{INT_NOM}) DURING DISCHARGE [a]

SOC	Cell #1	Cell #2	Cell #3	Cell #4
30%	10.5 ; 17.5	10.1 ; 17.4	10.4 ; 17.9	9.7 ; 17
70%	10.1 ; 15.5	10.1 ; 14.9	10.4 ; 15.4	9.6 ; 14.7
90%	10.2 ; 16.5	10.1 ; 14.8	10.3 ; 15.4	9.6 ; 14.5

a. Units are in mΩ. The Ro value specified by the datasheet is 10 mΩ

TABLE IV. INTERNAL RESISTANCE GROWTH DURING DISCHARGE AFTER 1400 CYCLES

SOC	Cell #1	Cell #2	Cell #3	Cell #4	Mean	σ
Ohmic internal resistance growth (R_o)						
30%	13,8%	12,4%	16,5%	14,9%	14,4%	1.7%
70%	21,4%	13,7%	17,3%	17,2%	17,4%	3%
90%	19,9%	15,4%	20,5%	19%	18,7%	2.3%
Total internal resistance growth ($R_{int} = R_o + R_p$)						
30%	18.6%	4.9%	5.3%	5.5%	8.6%	6.7%
70%	28.9%	17.3%	21.2%	16.8%	21.1%	5.59%
90%	28.7%	31%	48.3%	29.3%	34.3%	9.4%

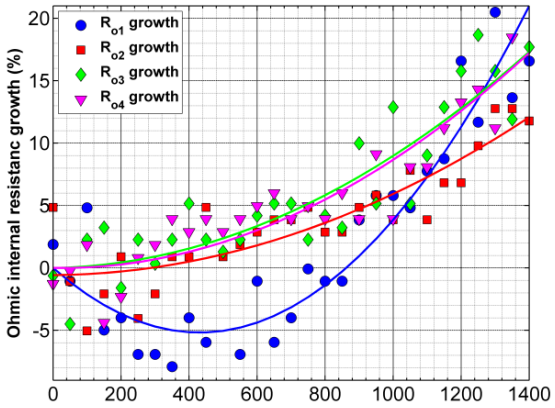

Fig. 11. R_o growth for 4 cell samples at SOC=70%.

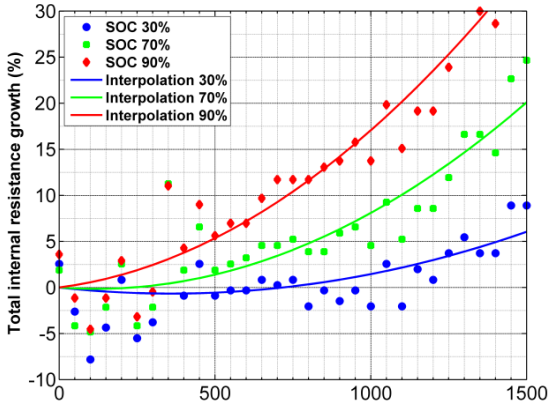

Fig. 12. R_{int} growth trend at SOC=70%. Cell sample #2.

V. CONCLUSION AND LIFETIME ESTIMATION

This work has implemented an accelerated ageing experiment to predict the lifetime of a battery pack embedded in a PHEV roadster, using a speed cycle as reference. Another purpose of this study was to observe the ageing behaviour of a PHEV design with high power requirements associated to low battery pack energy and compare the ageing results to other existing battery ageing models. The reported conclusion is that a high C-Rate peak, of up to 8 C, has a significant effect on the ageing behaviour when compared to the cell datasheet (table V). In fact, this results in a life expectancy that is 40% lower than reported in the cell datasheet. Because of the low battery pack energy, the proportion of the current peaks involved in the current battery pack design over typical values is high (see Fig. 9). From the experiment, we also conclude that the battery ageing process will affect both capacity and internal resistance. But the cell capacity will be reduced more rapidly, compared to the increase in internal resistance. Given an End Of Life (EOL) criteria of 20% loss in capacity, the EOL expected is reached after an average of 1426 cycles and 5564Ah exchanged by each of the cells, while the R_{int} growth stays lower than 14% (at 70% SOC) for the same number of WMTC cycles. Likewise, a notable disparity is observed between each cell ageing results and the mean results, when the standard deviation σ is considered (it reaches 16.6% for the capacity loss and more than 9% for the R_{int} growth). However, a part of these disparities can be associated to the measurable difference between each hardware control module.

TABLE V. AGEING ESTIMATION OF THE PHEV ROADSTER'S BATTERY PACK BASED ON MEAN RESULTS

Performance	Mid-life[a]			End-life[a]	
	Experiment		Datasheet	Experiment	
Number of WMTC[b]	600		1000	1150	
Capacity loss[%]	10		< 10%	20	
R_o & R_{int} growth [%]	R_o	R_{int}[d]		R_o	R_{int}[d]
SOC = 30%	2.6	-0.5		8.89	3.9
SOC = 70%	2.9	4.67		10.3	13.2
SOC = 90%	2.9	11.3		11.2	23.6
Ah-throughput [Ah]	3000		4370	5564	
Total distance [km]	27869			41354	
Lifetime [years][d]	4			6	

a. Mid-life reference is at 10% capacity loss and end-life reference is at 20% capacity loss respectively.

b. Considering the 24% Ah-throughput needed for the measures

c. The mean distance is 7000 km per year

d. $R_{int}=R_o+R_p$

Finally, for the PHEV roadster design, a lifetime prediction of about 41000 km or 5.9 years is computed, provided that the WMTC cycle is used at all time. Then, it can be concluded, from this experiment, that high current peaks, even if their cumulative distribution rate is low, accelerate significantly the ageing process, which decreases the vehicle performances and makes the use of common ageing models difficult.

REFERENCES

[1] Q. Badey, "Étude des mécanismes et modélisation du vieillissement des batteries lithium-ion dans le cadre d'un usage automobile," PhD thesis, 2012 (french).

[2] J. Wang, P. Liu, J. Hicks-Garner, E. Sherman, S. Soukiazian, M. Verbrugge, H. Tataria, J. Musser and P. Finamore, "Cycle-life model for graphite-LiFePO4 cells," J. Power Sources, vol. 196, pp. 3942-8, 04/15, 2011.

[3] V. Marano, S. Onori, Y. Guezennec, G. Rizzoni and N. Madella, "Lithium-ion batteries life estimation for plug-in hybrid electric vehicles," in 5th IEEE Vehicle Power and Propulsion Conference, VPPC '09, September 7, 2009 - September 10, 2009, pp. 536-543.

[4] N. Watrin, B. Blunier and A. Miraoui, "Review of adaptive systems for lithium batteries state-of-charge and state-of-health estimation," in Transportation Electrification Conference and Expo (ITEC), 2012 IEEE, 2012, pp. 1-6.

[5] J. Groot, "State-of-Health Estimation of Li-ion Batteries: Cycle Life Test Methods," Master thesis, 2012.

[6] N. Denis, M. Dubois and K. P. Angarita Gil, "Model development and performance estimation of a three-wheel plug-in hybrid electric vehicle," in EV2012VÉ, 2012, pp. 1-16.

[7] K. P. Angarita Gil, "Modélisation électrique et analyse d'une cellule lithium," master thesis, 2012 (french).

[8] X. Wei, B. Zhu and W. Xu, "Internal resistance identification in vehicle power lithium-ion battery and application in lifetime evaluation," in 2009 International Conference on Measuring Technology and Mechatronics Automation (ICMTMA), 2009, pp. 388-92.

[9] H. G. Schweiger, O. Obeidi, O. Komesker, A. Raschke, M. Schiemann, C. Zehner, Gehnen, M., Keller, M and P. Birke, " Comparison of Several Methods for Determining the Internal Resistance of Lithium Ion Cells ," Sensors, pp. 2011-5604-5625, 2010.

[10] D. Andrea, Battery Management Systems for Large Lithium-Ion Battery Packs. Boston: Artech House, 2010.